Study of $e^+e^- \to \eta\phi$ via initial state radiation at Belle

W. J. Zhu, B. S. Gao, X. L. Wang, I. Adachi, H. Aihara, D. M. Asner, H. Atmacan, T. Aushev, V. Babu, S. Bahinipati, P. Behera, K. Belous, J. Bennett, M. Bessner, V. Bhardwaj, T. Bilka, D. Bodrov, G. Bonvicini, J. Borah, A. Bozek, M. Bračko, P. Branchini, T. E. Browder, A. Budano, M. Campajola, D. Červenkov, M.-C. Chang, A. Chen, B. G. Cheon, K. Chilikin, H. E. Cho, K. Cho, S.-J. Cho, S.-K. Choi, Y. Choi, S. Choudhury, D. Cinabro, G. De Pietro, R. Dhamija, F. Di Capua, J. Dingfelder, Z. Doležal, T. V. Dong, D. Epifanov, D. Ferlewicz, B. G. Fulsom, V. Gaur, A. Garmash, A. Giri, P. Goldenzweig, E. Graziani, T. Gu, K. Gudkova, C. Hadjivasiliou, S. Halder, T. Hara, K. Hayasaka, H. Hayashii, C.-L. Hsu, K. Inami, N. Ipsita, A. Ishikawa, R. Itoh, M. Iwasaki, Y. Iwasaki, W. W. Jacobs, E.-J. Jang, Q. P. Ji, S. Jia, Y. Jin, K. K. Joo, K. H. Kang, C. Kiesling, C. H. Kim, D. Y. Kim, K.-H. Kim, Y.-K. Kim, K. Kinoshita, P. Kodyš, T. Konno, A. Korobov, S. Korpar, E. Kovalenko, P. Križan, P. Krokovny, M. Kumar, R. Kumar, K. Kumara, A. Kuzmin, Y.-J. Kwon, K. Lalwani, T. Lam, M. Laurenza, S. C. Lee, J. Li, L. K. Li, Y. Li, L. Li Gioi, J. Libby, K. Lieret, D. Liventsev, M. Masuda, T. Matsuda, D. Matvienko, S. K. Maurya, M. Merola, K. Miyabayashi, R. Mizuk, M. Nakao, A. Natochii, L. Nayak, M. Nayak, M. Niiyama, N. K. Nisar, S. Nishida, H. Ono, G. Pakhlova, S. Pardi, S.-H. Park, A. Passeri, S. Patra, S. Paul, T. K. Pedlar, R. Pestotnik, L. E. Piilonen, T. Podobnik, M. T. Prim, N. Rout, G. Russo, S. Sandilya, A. Sangal, L. Santelj, V. Savinov, G. Schnell, C. Schwanda, Y. Seino, K. Senyo, M. E. Sevior, M. Shapkin, C. Sharma, J.-G. Shiu, E. Solovieva, S. Stanič, M. Starič, Z. S. Stottler, J. F. Strube, M. Sumihama, T. Sumiyoshi, M. Takizawa, U. Tamponi, K. Tanida, F. Tenchini, K. Trabelsi, M. Uchida, T. Uglov, Y. Unno, S. Uno, P. Urquijo, Y. Usov, S. E. Vahsen, R. van Tonder, G. Varner, A. Vossen, E. Waheed, E. Wang, M.-Z. Wang, M. Watanabe, S. Watanuki, E. Won, W. Yan, S. B. Yang, J. H. Yin, C. Z. Yuan, Z. P. Zhang, V. Zhilich, and and V. Zhukova

(Belle Collaboration)

(Received 1 September 2022; accepted 10 October 2022; published 27 January 2023)

Using 980 fb^{-1} of data collected on and around the $\Upsilon(nS)$ ($n = 1, 2, 3, 4, 5$) resonances with the Belle detector at the KEKB collider, we measure the cross section of $e^+e^- \to \eta\phi$ from threshold to 3.95 GeV via initial state radiation. There are clear $\phi(1680)$ and J/ψ signals but no significant $\phi(2170)$ signal in the $\eta\phi$ final state. The branching fraction $\mathcal{B}[J/\psi \to \eta\phi]$ is measured to be $(7.2 \pm 0.8 \pm 0.5) \times 10^{-4}$. The resonant parameters of $\phi(1680)$ are determined to be $m_{\phi(1680)} = (1696 \pm 8 \pm 10)$ MeV/c^2 (statistical and systematic errors, respectively), $\Gamma_{\phi(1680)} = (175 \pm 13 \pm 16)$ MeV and, depending on the possible presence of predominantly constructive or destructive interference between $\phi(1680)$ and continuum production, $\Gamma^{e^+e^-}_{\phi(1680)} \cdot \mathcal{B}[\phi(1680) \to \eta\phi]$ and $\mathcal{B}[\phi(1680) \to \eta\phi]$ are determined to be $(75 \pm 10 \pm 11)$ eV and $(25 \pm 12 \pm 2)\%$ or $(207 \pm 16 \pm 20)$ eV and $(23 \pm 10 \pm 2)\%$, respectively. The upper limit for $\Gamma^{e^+e^-}_{\phi(2170)} \cdot \mathcal{B}[\phi(2170) \to \eta\phi]$ is determined to be either 0.17 or 18.6 eV at the 90% confidence level.

DOI: 10.1103/PhysRevD.107.012006

I. INTRODUCTION

Quarkonium and quarkoniumlike states play an important role in understanding quantum chromodynamics (QCD), which is the generally accepted theory for strong interactions between quarks and gluons. However, there are no first-principles methods to derive the spectrum and properties of hadrons from the QCD Lagrangian. Alternatively, the more phenomenological quark model is used comprehensively [1]. Although hadrons with multiple quarks ($n > 3$), with only gluons, or with bound hadrons, etc., are allowed according to QCD, only recently have accordant candidates been identified. Since the discovery of $X(3872)$ in 2003 by the Belle experiment [2], dozens of new states have been observed by Belle, *BABAR*, BESIII, CLEOc, LHCb, etc. However, these new states do not easily fit into the hadronic spectrum derived from the quark model, indicating that new types of hadrons may have already been observed. For example, the charged charmoniumlike states, such as $Z_c(3900)$ [3], $X(4020)^{\pm}$ [4] and $X(4055)^{\pm}$ [5,6], are generally interpreted as exotic states.

Hadronic transitions have contributed significantly to the discoveries of quarkonium(like) states, such as the $Y(4260)$ in $e^+e^- \to \pi^+\pi^- J/\psi$ via initial state radiation (ISR) by the *BABAR* experiment [7]. In searching for an $s\bar{s}$ version of the $Y(4260)$, the $Y(2175)$ [now called "$\phi(2170)$"] was discovered in $e^+e^- \to \pi^+\pi^-\phi$ via ISR by *BABAR* [8], and later confirmed by Belle [9]. There are several interpretations of the $\phi(2170)$, such as a regular $s\bar{s}$ meson [10,11], an $s\bar{s}g$ hybrid [12], a tetraquark state [13–15], a $\Lambda\bar{\Lambda}$ bound state [16–19], an S-wave threshold effect [20], or a three-meson system ϕKK [21]. In a recent lattice QCD calculation [22], the properties of the lowest two states comply with those of $\phi(1020)$ and $\phi(1680)$, but with no obvious correspondence to the $\phi(2170)$. In searching for $\phi(2170)$ in other hadronic transitions, *BABAR* studied the $e^+e^- \to \eta\phi$ process via ISR using a 232 fb^{-1} data sample and found several hundreds of $\eta\phi$ signal events, among which hints of an excess were observed around 2.1 GeV/c^2 [23,24]. Assuming these hints correspond to a bound ϕ'' state, *BABAR* estimated the mass $M_{\phi''} = (2125 \pm 22 \pm 10)$ MeV/c^2, width $\Gamma_{\phi''} = (61 \pm 50 \pm 13)$ MeV and product of the partial width times branching fraction $\Gamma^{e^+e^-}_{\phi''}\mathcal{B}[\phi'' \to \phi\eta] = (1.7 \pm 0.7 \pm 1.3)$ eV. (Hereinafter, quoted uncertainties are statistical and systematic, respectively.) The CMD-3 experiment measured the process $e^+e^- \to KK\eta$ from 1.59 to 2.007 GeV, found it is dominated by the $\eta\phi$ contribution, and then calculated the contribution to the anomalous magnetic moment of muon: $\alpha_\mu^{\eta\phi}(E < 1.8\ \text{GeV}) = (0.321 \pm 0.015 \pm 0.016) \times 10^{-10}$, $\alpha_\mu^{\eta\phi}(E < 2.0\ \text{GeV}) = (0.440 \pm 0.015 \pm 0.022) \times 10^{-10}$ [25]. Recently, BESIII measured $e^+e^- \to \phi\eta'$ with a data sample taken at center of mass (c.m.) energies ($\sqrt{s}$) ranging from 2.05 to 3.08 GeV and observed a resonance near 2.17 GeV with a statistical significance exceeding 10σ [26]. If both of these correspond to decays of the $\phi(2170)$, one could infer the ratio $\mathcal{B}[\phi(2170) \to \phi\eta]/\mathcal{B}[\phi(2170) \to \phi\eta'] = 0.23 \pm 0.10 \pm 0.18$, which is smaller than the prediction of $s\bar{s}g$ hybrid models by several orders of magnitude. However, due to limited statistics, the uncertainty in $\Gamma^{e^+e^-}_{\phi''}\mathcal{B}[\phi'' \to \phi\eta]$ from *BABAR* is large [24]. BESIII also measured the Born cross section of $e^+e^- \to \eta\phi$ and determined the $\phi(2170)$ parameters to be $m_{\phi(2170)} = (2163.5 \pm 6.2 \pm 3.0)$ MeV/c^2, $\Gamma_{\phi(2170)} = (31.1^{+21.1}_{-11.6} \pm 1.1)$ MeV, and $\Gamma^{e^+e^-}_{\phi(2170)}\mathcal{B}[\phi(2170) \to \phi\eta] = (0.24^{+0.12}_{-0.07})$ or $(10.11^{+3.87}_{-3.13})$ eV [27]. The signal significance of $\phi(2170)$ is determined to be 6.9σ. In that analysis, BESIII used, as input, the cross section of $e^+e^- \to \eta\phi$ below 2.0 GeV [dominated by the $\phi(1680)$ signal] measured by *BABAR* [24] in the determination of the $\phi(2170)$ resonant parameters.

In this article, we report a study of the $e^+e^- \to \eta\phi$ process via ISR with the Belle detector [28] at the KEKB asymmetric-energy e^+e^- collider [29]. The integrated luminosity used in this analysis is 980 fb^{-1}, of which ~70% were collected at the $\Upsilon(4S)$ resonance, with the remainder accumulated either at the other $\Upsilon(nS)$ ($n = 1, 2, 3, 5$) resonances or at $\sqrt{s}$ lower than the Υ resonances by tens of MeV. This data sample is much larger than the one used in the previous analyses [23,24]. We scan the $\phi(1680) \to \eta\phi$ final state over the energy interval from threshold to 3.95 GeV/c^2, which also covers the signal regions for $\phi(2170)$ and J/ψ. The well-improved precision of the cross section of $e^+e^- \to \eta\phi$ will be helpful to calculated the $\alpha_\mu^{\eta\phi}$ [30]. The ϕ is reconstructed from its decay to K^+K^- final state, and the η is reconstructed from its decay to either the $\gamma\gamma$ or $\pi^+\pi^-\pi^0$ final states.

II. THE BELLE DETECTOR AND MONTE CARLO (MC) SIMULATION

The Belle detector is a large-solid-angle magnetic spectrometer consisting of a silicon vertex detector, a 50-layer central drift chamber, an array of aerogel threshold Cherenkov counters, a barrel-like arrangement of time-of-flight scintillation counters, and an electromagnetic calorimeter (ECL) comprised of CsI(Tl) crystals located inside a superconducting solenoid coil that provides a 1.5 T magnetic field. An iron flux return located outside of the coil is instrumented to detect K^0_L mesons and to also identify muons. With the origin of the coordinate system defined as the nominal interaction point, the z axis is aligned with the direction opposite the e^+ beam and is parallel to the direction of the magnetic field within the solenoid. The y axis is vertical upward, and the x axis is horizontal and completes the right-handed coordinate frame. The polar angle θ and azimuthal angle ϕ are measured relative to the positive z and x axes, respectively.

The PHOKHARA event generator [31] is used to simulate the process $e^+e^- \to \eta\phi$ via ISR for optimization of selection criteria and the efficiency estimation. One or more ISR photons (γ_{ISR}) are emitted before forming a resonance Y, which then decays to $\eta\phi$ with $\phi \to K^+K^-$ and $\eta \to \pi^+\pi^-\pi^0$ or $\gamma\gamma$. In the generator, the resonance Y could be $\phi(1680)$, $\phi(2170)$, J/ψ or a particle with mass fixed to a value between the threshold and 3.95 GeV/c^2 and width fixed to zero to determine the efficiency and the mass resolution. Since the $\phi(1680)$ dominates the $\eta\phi$ final states, we use the MC sample of $\phi(1680)$ as the nominal signal MC sample. A GEANT3-based MC simulation [32] is used to simulate the Belle detector response.

III. EVENT SELECTION CRITERIA

To study the $\eta\phi$ final states, a ϕ candidate is reconstructed from a K^+K^- pair and an η candidate is reconstructed in either the $\gamma\gamma$ or $\pi^+\pi^-\pi^0$ ($\pi^0 \to \gamma\gamma$) modes. Hereinafter, the reconstruction channel with $\eta \to \gamma\gamma$ is called the "$\gamma\gamma$ mode," and the three-pion mode is referred to as the "$\pi^+\pi^-\pi^0$ mode." For a candidate event, we require

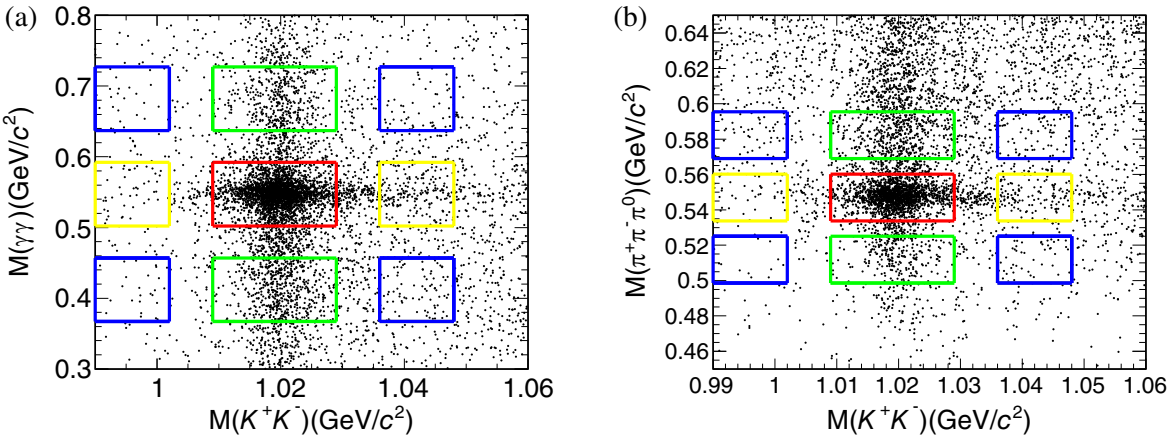

FIG. 1. Invariant mass distributions of (a) K^+K^- versus $\gamma\gamma$ and (b) K^+K^- versus $\pi^+\pi^-\pi^0$ for the selected $\pi^+\pi^-\pi^0K^+K^-$ or $\gamma\gamma K^+K^-$ candidates having $\eta\phi$ invariant mass below 3.5 GeV/c^2. The box in the center of each plot shows the $\eta\phi$ signal region, while the surrounding boxes show the sideband regions, defined according to the scheme described in the text.

two (four) well-measured charged tracks with zero net charge for the $\gamma\gamma$ ($\pi^+\pi^-\pi^0$) mode. A well-measured charged track is defined as one having impact parameters with respect to the interaction point satisfying $\delta r < 1.5$ cm in the $r-\phi$ plane and $\delta z < 5$ cm in the r–z plane, respectively. For each charged track, information from different detector subsystems is combined to form a likelihood $\mathcal{L}_i$ for each putative particle species (i) [33]. Tracks with $\mathcal{R}_K = \frac{\mathcal{L}_K}{\mathcal{L}_K+\mathcal{L}_\pi} > 0.6$ are identified as kaons, while those with $\mathcal{R}_K < 0.4$ are identified as pions, with an efficiency of about 95% for $K-\pi$ separation.

Each photon candidate is a cluster in the ECL that is unmatched to the extrapolated trajectories of any charged tracks. The photon with the highest energy is identified to be $\gamma_{\rm ISR}$. In the reconstruction of π^0 candidates, the energy of a photon candidate is required to have $E_\gamma > 25$ MeV in the barrel ($\cos\theta \in [-0.63, 0.85]$) and $E_\gamma > 50$ MeV in the end caps ($\cos\theta \in [-0.91, -0.65] \cup [0.85, 0.98]$). The $M_{\gamma\gamma}$ mass resolution is about 6 MeV/c^2, and the signal region of the π^0 is defined to be $120 < M_{\gamma\gamma} < 150$ MeV/c^2 with $\chi^2(\pi^0) < 25$ (the χ^2 value returned for the mass fit to each π^0 candidate). Events with $\gamma \to e^+e^-$ conversions are removed by requiring $\mathcal{R}_e < 0.75$ for the $\pi^+\pi^-$ tracks from η decays. In this case, the particle identification variable for electron/positron in conversion products is defined as $\mathcal{R}_e \equiv \mathcal{L}_e/(\mathcal{L}_e + \mathcal{L}_{\rm hadrons})$. In the reconstruction of $\eta \to \gamma\gamma$, two photon candidates are required, each with energy satisfying $E_{\gamma_l} > 120$ MeV and $E_{\gamma_h} > 350$ MeV, where the subscript l (h) signifies the lower (higher) energy photon in the laboratory system. The efficiency of the energy requirement is $(96.6 \pm 0.1)\%$ (statistical error only), as determined from signal MC simulation.

The scatter plots displaying the dikaon ($M_{K^+K^-}$) invariant mass versus the $\pi^+\pi^-\pi^0$ invariant mass ($M_{\pi^+\pi^-\pi^0}$) or the $\gamma_l\gamma_h$ invariant mass ($M_{\gamma\gamma}$) are shown in Fig. 1, and the 1D projections are shown in Fig 2. A K^+K^- pair is treated as a ϕ candidate if $|M_{K^+K^-} - m_\phi| < 12$ MeV/c^2 (the mass resolution is ~4 MeV/c^2), where m_ϕ is the ϕ nominal mass [34]. This mass interval requirement for the ϕ retains $(97.1 \pm 0.6)\%$ of ϕ candidates in data and $(97.4 \pm 0.1)\%$ in the signal MC simulation, respectively. The lower and upper ϕ mass sidebands are defined to be $0.990 < M_{K^+K^-} < 1.002$ GeV/c^2 and $1.036 < M_{K^+K^-} < 1.048$ GeV/c^2, respectively. A fit to the $M_{\pi^+\pi^-\pi^0}$ or $M_{\gamma\gamma}$ distribution with a Gaussian function for the η signal and a smooth second-order polynomial function for background yields a mass resolution of $\sigma_{\pi^+\pi^-\pi^0} = 4.2$ MeV/c^2 in the $\pi^+\pi^-\pi^0$ mode and $\sigma_{\gamma\gamma} = 11.3$ MeV/c^2 in the $\gamma\gamma$ mode. We define the η

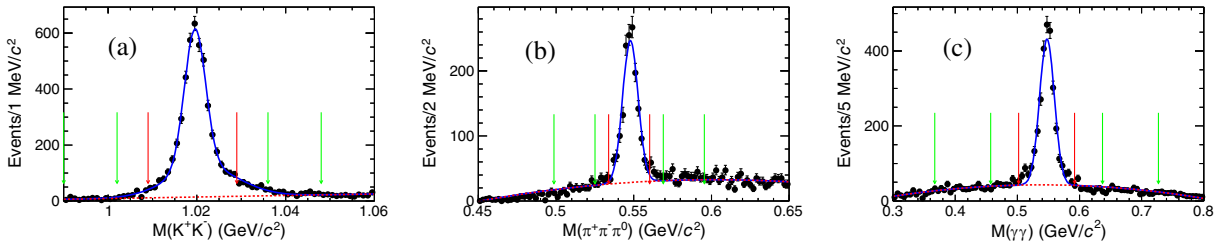

FIG. 2. Invariant mass distributions of (a) K^+K^- for ϕ signal, (b) $\pi^+\pi^-\pi^0$ and (c) $\gamma\gamma$ for η signal from data. The curves show the best-fit results with Gaussian functions for ϕ and η signals and second-order polynomial functions for backgrounds. The red arrows show the signal regions and the green arrows show the sideband regions.

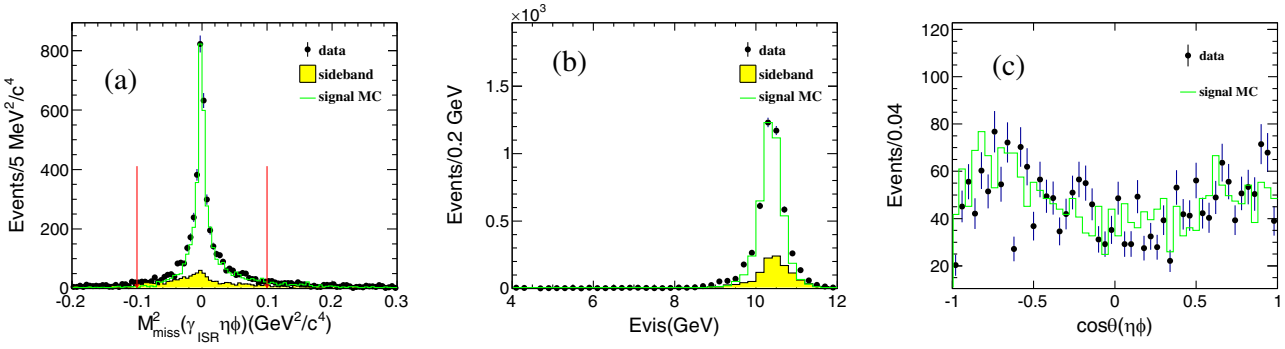

FIG. 3. The ISR characteristics of the final states. Plot (a) shows the missing mass squared of $\eta\phi$ and $\gamma_{\rm ISR}$, (b) shows the visible energy in the detector and (c) shows the angular distribution of $\eta\phi$ in the e^+e^- c.m. frame. The dots with error bars correspond to data while the shaded histograms correspond to backgrounds estimated from the 2D sidebands. The blank histograms are the signal MC simulations, with the highest bin content normalized to that of the data. In plot (c), the backgrounds estimated from 2D sidebands have been subtracted from the data.

signal mass interval by $|M_{\pi^+\pi^-\pi^0/\gamma\gamma} - m_\eta| < 3\sigma_{\pi^+\pi^-\pi^0/\gamma\gamma}$, and the sideband regions are defined by $|M_{\pi^+\pi^-\pi^0} - m_\eta \pm 9\sigma_{\pi^+\pi^-\pi^0/\gamma\gamma}| < 3\sigma_{\pi^+\pi^-\pi^0/\gamma\gamma}$, where m_η is the nominal η mass 34]]. The central (surrounding) rectangles of Fig. 1 show the $\eta\phi$ signal (sideband) regions. With $S1$, $S2$ and $S3$ representing the sum of the events in the two adjacent horizontal ($S1$) and vertical ($S2$) sideband boxes and ($S3$) the four diagonal sideband boxes relative to the signal box, the normalization of the two-dimensional (2D) sidebands is given by $S = a \cdot S1 + b \cdot S2 - ab \cdot S3$, where $a = 0.84 \pm 0.05$ and $b = 0.52 \pm 0.03$ are the appropriate areal scale factors, according to the $M_{K^+K^-}$ and $M_{\pi^+\pi^-\pi^0/\gamma\gamma}$ distributions. These 2D sidebands are used to estimate the background level in the $\eta\phi$ signal region.

For most of the ISR events, the missing mass squared of the reconstructed η, ϕ, and $\gamma_{\rm ISR}$ candidates $[M^2_{\rm miss}(\gamma_{\rm ISR}\eta\phi)]$ is close to zero, consistent with either complete reconstruction or a low-energy, second ISR photon eluding detection [Fig. 3(a)]. We also require $|M^2_{\rm miss}(\gamma_{\rm ISR}\eta\phi)| < 0.1\ {\rm GeV}^2/c^4$ with a mass-selection efficiency of $(97.7 \pm 0.3)\%$ in the $\pi^+\pi^-\pi^0$ mode and $(97.1 \pm 0.3)\%$ in the $\gamma\gamma$ mode. Figures 3(b) and 3(c) illustrate the good agreement between data and signal MC simulations for the distributions of visible energy of all final state photons and charged particles ($E_{\rm vis}$), as well as the polar angle of the $\eta\phi$ system in the e^+e^- c.m. frame [$\cos\theta(\eta\phi)$], confirming that the signal events are produced via ISR.

IV. INVARIANT MASS SPECTRUM OF $\eta\phi$ FROM ISR PRODUCTION

After imposing the selection criteria, the distributions of the $\eta\phi$ invariant mass ($M_{\eta\phi}$) from the two modes are shown in Fig. 4, together with the backgrounds estimated from the scaled 2D sidebands. Using $M_{\eta\phi} \equiv M_{\pi^+\pi^-\pi^0K^+K^-} - M_{\pi^+\pi^-\pi^0} - M_{K^+K^-} + m_\eta + m_\phi$ for the $\eta \to \pi^+\pi^-\pi^0$ mode and $M_{\eta\phi} \equiv M_{\gamma\gamma K^+K^-} - M_{\gamma\gamma} - M_{K^+K^-} + m_\eta + m_\phi$ for the $\eta \to \gamma\gamma$ mode, the mass resolution of $\eta\phi$ is about 6 MeV/c^2. The number of obtained $\eta\phi$ signal events is about 7 times larger than the previous work [23,24], although there is not an obvious ϕ'' signal.

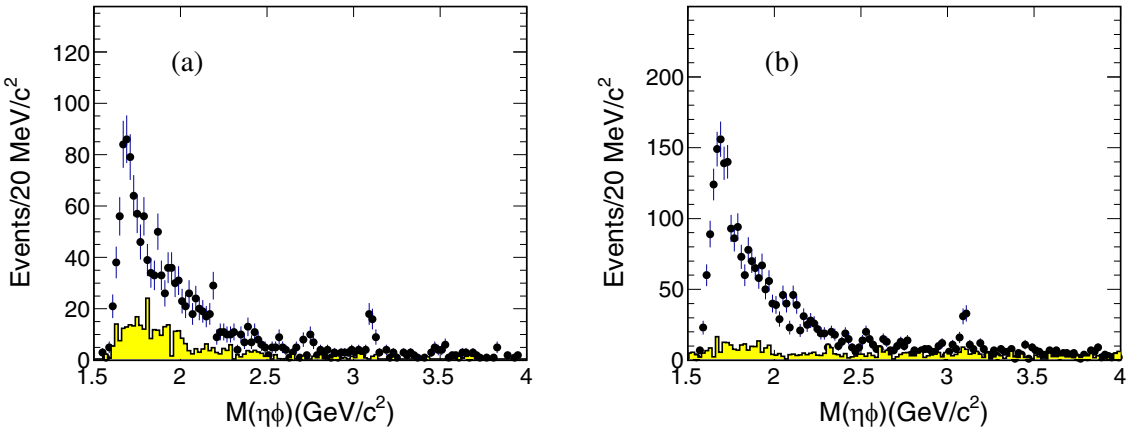

FIG. 4. Invariant mass $\eta\phi$ distributions in (a) the $\pi^+\pi^-\pi^0$ mode and (b) the $\gamma\gamma$ mode from data. The points with error bars are from the signal region and the shaded histograms are backgrounds estimated from the 2D sidebands.

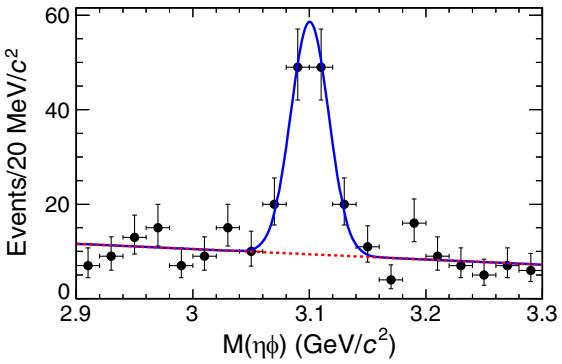

FIG. 5. The J/ψ signal in the combined $M_{\eta\phi}$ spectrum of the $\pi^+\pi^-\pi^0$ mode and the $\gamma\gamma$ mode from data. The curves shows the best-fit results. The blue curve is a Gaussian function for the J/ψ signal, and the dashed line is a second-order polynomial function for the backgrounds.

There are clear J/ψ signals in both the $\pi^+\pi^-\pi^0$ mode and the $\gamma\gamma$ mode. As shown in Fig. 5, an unbinned maximum likelihood fit is performed to the combined $M_{\eta\phi}$ spectrum of the two modes, with a Gaussian function with the resolution fixed to the signal MC simulation for the J/ψ signals and a second-order polynomial function for the backgrounds. The J/ψ signal yield is $N_{\rm sig}^{\rm fit} = (100 \pm 12)$. To estimate the fitting systematic error, polynomial functions of either first or third order are also used for the background parametrization. The branching fraction for the $J/\psi \to \eta\phi$ decay is calculated using

$$\mathcal{B}(J/\psi \to \eta\phi) = \frac{N_{\rm sig}^{\rm fit}}{\sigma_{\rm ISR}^{\rm prod} \times \mathcal{L} \times \varepsilon \times \mathcal{B}[\phi \to K^+K^-] \times \mathcal{B}[\eta \to \gamma\gamma/\pi^+\pi^-\pi^0]}, \quad (1)$$

where $\mathcal{L}$, ε, $\mathcal{B}[\phi \to K^+K^-]$, and $\mathcal{B}[\eta \to \gamma\gamma/\pi^+\pi^-\pi^0]$ are the integrated luminosity of the Belle data sample, the detection efficiency, the $\phi \to K^+K^-$ branching fraction, and the combined branching fraction for the $\eta \to \gamma\gamma$ and $\pi^+\pi^-\pi^0$ final states [34], respectively; $\sigma_{\rm ISR}^{\rm prod}(J/\psi) = (37.5 \pm 0.2)$ pb is the cross section for J/ψ production via ISR for the Belle experiment [9]. With systematic uncertainties as described below in Sec. VI, the branching fraction of $J/\psi \to \eta\phi$ is measured to be $(7.2 \pm 0.8 \pm 0.5) \times 10^{-4}$, which agrees well with the world average value of $(7.4 \pm 0.8) \times 10^{-4}$ [34].

We observe a clear $\phi(1680)$ signal in the $\eta\phi$ final state. However, the $\phi(2170)$ is not as prominent as in the previous BESIII [27] analysis. An unbinned maximum likelihood fit is performed to the $M_{\eta\phi}$ mass spectra from threshold to 2.85 GeV/c^2 using signal candidate events and 2D sideband events, simultaneously. Similar to the parametrization in *BABAR*'s measurement [24], the parametrization for the cross section of $e^+e^- \to \eta\phi$ at $\sqrt{s}$ takes the form

$$\sigma_{\eta\phi}(\sqrt{s}) = 12\pi\mathcal{P}_{\eta\phi}(\sqrt{s})|A_{\eta\phi}^{n.r.}(\sqrt{s}) + A_{\eta\phi}^{\phi(1680)}(\sqrt{s}) + A_{\eta\phi}^{\phi(2170)}(\sqrt{s})|^2, \quad (2)$$

where $\mathcal{P}_{\eta\phi}$ is the phase space of the final state, $A_{\eta\phi}^{n.r.}(\sqrt{s}) = a_0/s^{a_1}$ describes the nonresonant contribution (mainly due to the tails of resonances below threshold), and $A_{\eta\phi}^{\phi(1680)}$ ($A_{\eta\phi}^{\phi(2170)}$) is the $\phi(1680)$ [$\phi(2170)$] amplitude. The $\phi(1680)$ resonance amplitude is described by a Breit-Wigner function

$$A_{\eta\phi}^{\phi(1680)}(\sqrt{s}) = \sqrt{\mathcal{B}_{\phi(1680)}^{\eta\phi}\Gamma_{\phi(1680)}^{e^+e^-}} \times \frac{\sqrt{\Gamma_{\phi(1680)}/\mathcal{P}_{\eta\phi}(M_{\phi(1680)}^2)}e^{i\theta_{\phi(1680)}}}{M_{\phi(1680)}^2 - s - i\sqrt{s}\Gamma_{\phi(1680)}(\sqrt{s})}, \quad (3)$$

where $M_{\phi(1680)}$, $\Gamma_{\phi(1680)}$ and $\Gamma_{\phi(1680)}^{e^+e^-}$ are the mass, the total width and the partial width to e^+e^- for the $\phi(1680)$, respectively. $\mathcal{B}_{\phi(1680)}^{\eta\phi}$ is the branching fraction $\mathcal{B}[\phi(1680) \to \eta\phi]$ and $\theta_{\phi(1680)}$ is the relative phase. As shown in *BABAR*'s measurement [24], several major decays of $\phi(1680)$ contribute to $\Gamma_{\phi(1680)}$, such as $KK^*(892)$ and $\eta\phi$. Since $\mathcal{B}_{\phi(1680)}^{KK^*(892)} \approx 2 \times \mathcal{B}_{\phi(1680)}^{\eta\phi}$, the phase space effect of $KK^*(892)$ cannot be ignored in describing $\Gamma_{\phi(1680)}$. Therefore, we take the form as in Ref [24]:

$$\Gamma_{\phi(1680)}(\sqrt{s}) = \Gamma_{\phi(1680)}\left[\frac{\mathcal{P}_{KK^*(892)}(\sqrt{s})}{\mathcal{P}_{KK^*(892)}(M_{\phi(1680)})}\mathcal{B}_{\phi(1680)}^{KK^*(892)} + \frac{\mathcal{P}_{\eta\phi}(\sqrt{s})}{\mathcal{P}_{\eta\phi}(M_{\phi(1680)})}\mathcal{B}_{\phi(1680)}^{\eta\phi} + \left(1 - \mathcal{B}_{\phi(1680)}^{\eta\phi} - \mathcal{B}_{\phi(1680)}^{KK^*(892)}\right)\right]. \quad (4)$$

Here, $\mathcal{P}_{KK^*(892)}$ and $\mathcal{B}_{\phi(1680)}^{KK^*(892)}$ are the phase space and branching fraction of the $\phi(1680) \to KK^*(892)$ decay, respectively. The other decays of $\phi(1680)$ are neglected, and their phase space dependence correspondingly ignored. Since both the $KK^*(892)$ and the $\eta\phi$ contain a vector meson (V) and a pseudoscalar meson (P), the phase space takes the form

$$\mathcal{P}_{VP}(\sqrt{s}) = \left[\frac{(s + M_V^2 - M_P^2)^2 - 4M_V^2 s}{s}\right]^{3/2}. \quad (5)$$

Since there is no measurement of the $KK^*(892)$ final state in this work, we take $\mathcal{B}^{\eta\phi}_{\phi(1680)}/\mathcal{B}^{KK^*(892)}_{\phi(1680)}$ directly from Ref. [24].

The $A^{\phi(2170)}_{\eta\phi}$ is described by

$$A^{\phi(2170)}_{\eta\phi}(s) = \sqrt{\mathcal{B}^{\eta\phi}_{\phi(2170)}\Gamma^{e^+e^-}_{\phi(2170)}} \times \frac{\sqrt{\Gamma_{\phi(2170)}/\mathcal{P}_{\eta\phi}(M^2_{\phi(2170)})}e^{i\theta_{\phi(2170)}}}{M^2_{\phi(2170)} - s - i\sqrt{s}\Gamma_{\phi(2170)}} \cdot \frac{B(p)}{B(p')}, \quad (6)$$

where $B(p)$ is the P-wave Blatt-Weisskopf form factor and p (p') is the breakup momentum corresponding to the $\sqrt{s}$ ($M_{\phi(2170)}$).

The efficiencies of the $M_{\eta\phi}$ signal selection are determined from MC samples generated in the range from threshold to 3.95 GeV/c^2 and are found to be about 1.35% over this mass interval. The effective integrated luminosity of ISR is calculated according to the theoretical prescription from [35], corresponding to 45 pb^{-1} per 10 MeV near 1.65 GeV and increasing to about 80 pb^{-1} per 10 MeV near 3.95 GeV. The 2D sideband events from S_1, S_2 and S_3 are described by three Landau functions; exponential functions are considered to estimate the systematic uncertainty.

Assuming the existence of $\phi(2170)$ in the $\eta\phi$ final state, and fitting using the mass and width of $\phi(2170)$ reported by BESIII [27], there are four solutions of equivalent quality, having the same $M_{\phi(1680)}$ and $\Gamma_{\phi(1680)}$. The fit results are shown in Fig. 6 and Table I. The reduced chi squared of the fit to the $M_{\eta\phi}$ spectrum is $\chi^2/ndf = 77/56$. The $\phi(1680)$ resonant parameters are determined to be $M_{\phi(1680)} = (1683 \pm 7 \pm 9)$ MeV/c^2, $\Gamma_{\phi(1680)} = (149 \pm 12 \pm 13)$ MeV, and $\mathcal{B}^{\eta\phi}_{\phi(1680)}\Gamma^{e^+e^-}_{\phi(1680)} = (122 \pm 6 \pm 13)$, $(219 \pm 15 \pm 18)$, $(163 \pm 11 \pm 13)$ or $(203 \pm 12 \pm 18)$ eV for the four solutions. The branching fraction $\mathcal{B}[\phi(1680) \to \eta\phi]$ obtained from the fit is $(18 \pm 2 \pm 1)\%$, $(19 \pm 4 \pm 2)\%$, $(21 \pm 2 \pm 1)\%$ or $(17 \pm 4 \pm 2)\%$ for the four solutions. The statistical significance of $\phi(2170)$ is determined to be 1.7σ by comparing the value of $\Delta(-2\ln\mathcal{L}) = -2\ln(\mathcal{L}_{\rm max}/\mathcal{L}_0)$ and the change in the number of free parameters in the fits, where $\mathcal{L}_{\rm max}$ is the likelihood with $\phi(2170)$ and $\mathcal{L}_0$ without $\phi(2170)$. The quantity $\Gamma^{e^+e^-}_{\phi(2170)}\mathcal{B}[\phi(2170) \to \eta\phi]$ is determined to be (0.09 ± 0.05), (0.06 ± 0.02), (16.7 ± 1.2) or (17.0 ± 1.2) eV in the four solutions. The upper limit for $\phi(2170)$ production at 90% confidence level (CL) is determined by integrating the likelihood versus the $\phi(2170)$ yield, with the upper limit degraded by a factor of $1/(1-\delta_{\rm sys})$ to account for systematic uncertainties. (The systematic uncertainties in the fit results and $\delta_{\rm sys}$ are described below in Sec. VI.) Finally, the upper limits for $\Gamma^{e^+e^-}_{\phi(2170)}\mathcal{B}[\phi(2170) \to \eta\phi]$ are determined to be 0.17 (solutions I and II) or 18.6 eV (solutions III and IV) at 90% CL, respectively.

Since the $\phi(2170)$ is not significant in our measurement, another fit without $\phi(2170)$ in Eq. (2) is performed, and there are two solutions as also indicated in Table I. There is no obvious difference in quality between the curves from fits with or without $\phi(2170)$. Including the systematic uncertainties, the resonant parameters of $\phi(1680)$ are obtained to be $m_{\phi(1680)} = (1696 \pm 8 \pm 10)$ MeV/c^2,

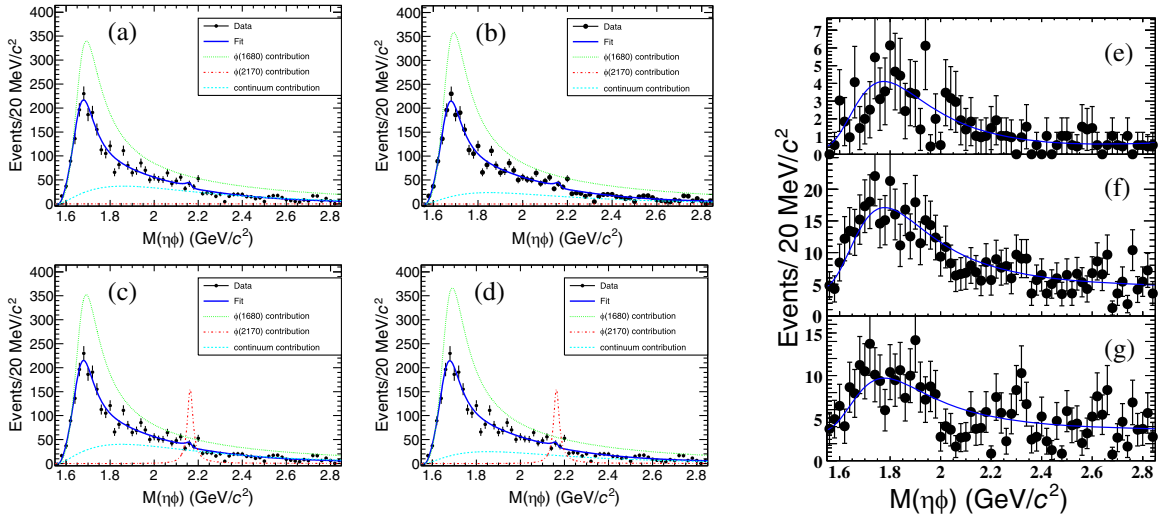

FIG. 6. Invariant mass distribution of $M(\eta\phi)$ and fit results. (a)–(d) show the four solutions, and (e)–(g) show the backgrounds estimated from 2D sidebands. In (a)–(d), the backgrounds estimated from 2D sidebands have been subtracted. The distribution in (e) shows events from the sideband region S_3, (f) from S_2 and (g) from S_1, respectively. The curves show the best-fit results, while the interference among continuum, $\phi(1680)$ and $\phi(2170)$ are not shown.

TABLE I. Fit results with $\phi(1680)$ and $\phi(2170)$ both included and also excluding $\phi(2170)$. The mass and width of $\phi(2170)$ are fixed from the prior BESIII measurement [27].

Parameters	With $\phi(2170)$				Without $\phi(2170)$	
	Solution I	Solution II	Solution III	Solution IV	Solution I	Solution II
χ^2/ndf	77/56				85/60	
a_0	-4.1 ± 0.5	5.0 ± 0.7	-5.0 ± 0.5	-4.8 ± 0.2	-3.2 ± 0.7	5.0 ± 0.1
a_1	2.7 ± 0.1	2.6 ± 0.1	2.7 ± 0.1	2.6 ± 0.1	2.9 ± 0.1	2.6 ± 0.1
$\Gamma^{\phi(1680)}_{e^+e^-}\mathcal{B}^{\phi(1680)}_{\eta\phi}$(eV)	122 ± 6	219 ± 15	163 ± 11	203 ± 12	75 ± 10	207 ± 16
$M_{\phi(1680)}$(MeV/c^2)	1683 ± 7				1696 ± 8	
$\Gamma_{\phi(1680)}$(MeV)	149 ± 12				175 ± 13	
$\mathcal{B}^{\phi(1680)}_{\eta\phi}$	0.18 ± 0.02	0.19 ± 0.04	0.21 ± 0.02	0.17 ± 0.04	0.25 ± 0.12	0.23 ± 0.10
$\Gamma^{\phi(2170)}_{e^+e^-}\mathcal{B}^{\phi(2170)}_{\eta\phi}$(eV)	0.09 ± 0.05	0.06 ± 0.02	16.7 ± 1.2	17.0 ± 1.2	…	
$M_{\phi(2170)}$(MeV/c^2)	2163.5 (fixed)				…	
$\Gamma_{\phi(2170)}$(MeV)	31.1 (fixed)				…	
$\theta_{\phi(1680)}(^\circ)$	-89 ± 2	96 ± 6	-92 ± 1	-86 ± 7	-87 ± 15	108 ± 22
$\theta_{\phi(2170)}(^\circ)$	37 ± 14	-102 ± 11	-167 ± 6	-155 ± 5	…	

$\Gamma_{\phi(1680)} = (175 \pm 13 \pm 16)$ MeV, $\Gamma^{e^+e^-}_{\phi(1680)}\mathcal{B}[\phi(1680) \to \eta\phi] = (75 \pm 10 \pm 11)$ eV or $(207 \pm 16 \pm 20)$ eV, and the branching fraction $\mathcal{B}[\phi(1680) \to \eta\phi] = (25 \pm 12 \pm 2)\%$ or $(23 \pm 10 \pm 2)\%$ depending on the interference between $\phi(1680)$ and continuum production for the two solutions.

V. CROSS SECTION FOR $e^+e^- \to \eta\phi$

The $M_{\eta\phi}$ distributions in Fig. 4 are combined and the cross section of $e^+e^- \to \eta\phi$ for each $M_{\eta\phi}$ bin with a width of 20 MeV/c^2 is calculated according to

$$\sigma_i = \frac{n_i^{\rm obs} - n_i^{\rm bkg}}{\mathcal{L}_i^{\rm ISR} \times \mathcal{B}[\phi \to K^+K^-] \times \sum_j \varepsilon_{ij}\mathcal{B}_j}, \qquad (7)$$

where i is the ith bin of the combined $M_{\eta\phi}$ distribution and j is the jth η decay mode; $n_i^{\rm obs}$, $n_i^{\rm bkg}$, $\mathcal{L}_i^{\rm ISR}$, ε_{ij} and $\mathcal{B}_j$ are the number of events observed in data, the number of background events estimated from the 2D sidebands, the effective integrated luminosity of ISR production in Belle data, the efficiency of signal selection, and the branching fraction of the jth η decay mode [34], respectively. The cross sections for $e^+e^- \to \eta\phi$ measured with Belle data are shown in Fig. 7 and Table II, where the error bars include the statistical uncertainties and the systematic uncertainties in the background estimation using the 2D sidebands. The cross sections for $e^+e^- \to \eta\phi$ are around 2.6 and 0.4 nb at the $\phi(1680)$ and $\phi(2170)$ peaks, respectively. The measured cross section is in good agreement with the results from *BABAR*'s measurement [23,24] but with improved precision.

VI. SYSTEMATIC UNCERTAINTIES

The following systematic uncertainties are characterized for this analysis. The uncertainties due to the particle identification are 2.0% in the $\gamma\gamma$ mode and 4.0% in $\pi^+\pi^-\pi^0$, respectively [33]. The uncertainty due to the tracking efficiency is 0.35% per track and is additive; the uncertainty in the photon reconstruction is 2% per photon. The uncertainties in the ϕ mass, η mass, and $M^2_{\rm miss}(\gamma_{\rm ISR}\eta\phi)$ requirements are measured with the control sample $e^+e^- \to J/\psi \to \eta\phi$; 1.3% for the η mass window is taken as a conservative uncertainty for the combined $\pi^+\pi^-\pi^0$ and $\gamma\gamma$ modes. For the ϕ mass window, the corresponding value is 0.5%. Similarly, 1.3% is taken to

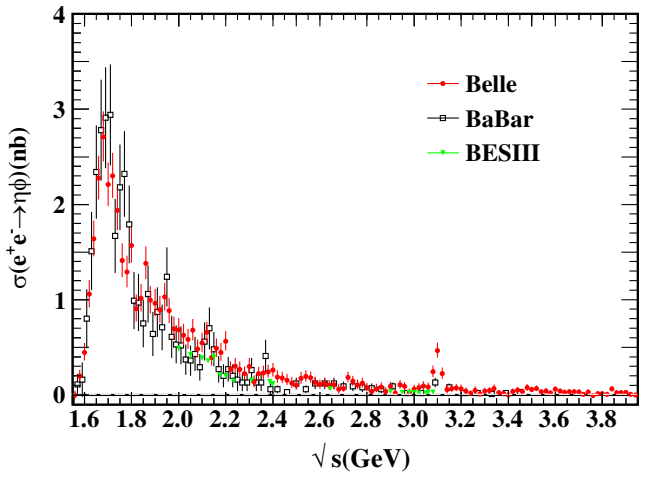

FIG. 7. Cross section for $e^+e^- \to \eta\phi$ from threshold to 3.95 GeV. The errors are the combinations of statistical errors and the systematic uncertainties.

TABLE II. Measured cross section of $e^+e^- \to \eta\phi$ from the threshold to $\sqrt{s} = 3.95$ GeV. The first errors are statistical and the second ones are systematic.

$\sqrt{s}$	$\sigma(e^+e^- \to \eta\phi)$	$\sqrt{s}$	$\sigma(e^+e^- \to \eta\phi)$	$\sqrt{s}$	$\sigma(e^+e^- \to \eta\phi)$	$\sqrt{s}$	$\sigma(e^+e^- \to \eta\phi)$
1.56	$-11^{+37}_{-45} \pm 16$	2.26	$236^{+69}_{-78} \pm 19$	2.96	$88^{+34}_{-44} \pm 6$	3.66	$31^{+23}_{-31} \pm 2$
1.58	$174^{+58}_{-70} \pm 15$	2.28	$182^{+63}_{-77} \pm 16$	2.98	$26^{+34}_{-42} \pm 2$	3.68	$31^{+21}_{-29} \pm 2$
1.60	$414^{+81}_{-95} \pm 28$	2.30	$256^{+73}_{-83} \pm 23$	3.00	$61^{+33}_{-47} \pm 4$	3.70	$31^{+19}_{-27} \pm 2$
1.62	$1004^{+119}_{-128} \pm 68$	2.32	$96^{+57}_{-69} \pm 6$	3.02	$77^{+36}_{-47} \pm 10$	3.72	$6^{+15}_{-22} \pm 1$
1.64	$1563^{+148}_{-156} \pm 107$	2.34	$180^{+60}_{-74} \pm 7$	3.04	$94^{+41}_{-50} \pm 10$	3.74	$30^{+20}_{-29} \pm 2$
1.66	$2191^{+170}_{-179} \pm 149$	2.36	$190^{+58}_{-72} \pm 13$	3.06	$85^{+38}_{-48} \pm 10$	3.76	$-6^{+9}_{-21} \pm 1$
1.68	$2600^{+186}_{-194} \pm 179$	2.38	$200^{+63}_{-70} \pm 17$	3.08	$243^{+52}_{-63} \pm 19$	3.78	$12^{+18}_{-24} \pm 1$
1.70	$2088^{+170}_{-179} \pm 143$	2.40	$220^{+63}_{-78} \pm 21$	3.10	$466^{+71}_{-77} \pm 32$	3.80	$12^{+18}_{-24} \pm 1$
1.72	$2157^{+173}_{-185} \pm 150$	2.42	$156^{+57}_{-65} \pm 15$	3.12	$223^{+53}_{-62} \pm 17$	3.82	$6^{+17}_{-21} \pm 1$
1.74	$1785^{+164}_{-172} \pm 126$	2.44	$145^{+52}_{-66} \pm 15$	3.14	$57^{+33}_{-39} \pm 9$	3.84	$63^{+22}_{-30} \pm 4$
1.76	$1257^{+140}_{-153} \pm 93$	2.46	$124^{+51}_{-67} \pm 8$	3.16	$65^{+37}_{-44} \pm 9$	3.86	$22^{+17}_{-23} \pm 1$
1.78	$1137^{+133}_{-148} \pm 94$	2.48	$92^{+43}_{-56} \pm 13$	3.18	$72^{+35}_{-41} \pm 9$	3.88	$22^{+16}_{-23} \pm 1$
1.80	$1414^{+148}_{-163} \pm 107$	2.50	$72^{+51}_{-56} \pm 11$	3.20	$64^{+29}_{-40} \pm 9$	3.90	$27^{+15}_{-24} \pm 6$
1.82	$751^{+118}_{-133} \pm 64$	2.52	$153^{+51}_{-65} \pm 10$	3.22	$39^{+29}_{-36} \pm 8$	3.92	$5^{+11}_{-19} \pm 1$
1.84	$873^{+121}_{-134} \pm 71$	2.54	$172^{+55}_{-62} \pm 12$	3.24	$16^{+25}_{-38} \pm 7$	3.94	$0^{+11}_{-16} \pm 0$
1.86	$1249^{+138}_{-152} \pm 93$	2.56	$161^{+51}_{-61} \pm 11$	3.26	$46^{+25}_{-35} \pm 8$		
1.88	$874^{+123}_{-130} \pm 67$	2.58	$120^{+45}_{-54} \pm 13$	3.28	$8^{+19}_{-30} \pm 7$		
1.90	$829^{+127}_{-133} \pm 61$	2.60	$100^{+44}_{-57} \pm 12$	3.30	$38^{+30}_{-38} \pm 8$		
1.92	$774^{+115}_{-129} \pm 58$	2.62	$109^{+47}_{-62} \pm 12$	3.32	$45^{+26}_{-32} \pm 8$		
1.94	$917^{+121}_{-130} \pm 66$	2.64	$89^{+48}_{-55} \pm 12$	3.34	$67^{+25}_{-36} \pm 8$		
1.96	$784^{+116}_{-124} \pm 58$	2.66	$98^{+52}_{-57} \pm 6$	3.36	$22^{+25}_{-36} \pm 5$		
1.98	$607^{+108}_{-116} \pm 48$	2.68	$49^{+29}_{-41} \pm 10$	3.38	$15^{+24}_{-31} \pm 7$		
2.00	$595^{+99}_{-113} \pm 43$	2.70	$58^{+38}_{-46} \pm 11$	3.40	$-7^{+17}_{-24} \pm 7$		
2.02	$540^{+98}_{-107} \pm 36$	2.72	$173^{+50}_{-63} \pm 15$	3.42	$29^{+25}_{-32} \pm 7$		
2.04	$506^{+91}_{-103} \pm 36$	2.74	$134^{+43}_{-53} \pm 13$	3.44	$42^{+28}_{-36} \pm 8$		
2.06	$615^{+93}_{-106} \pm 43$	2.76	$95^{+48}_{-53} \pm 12$	3.46	$28^{+19}_{-30} \pm 7$		
2.08	$417^{+84}_{-96} \pm 28$	2.78	$113^{+45}_{-53} \pm 8$	3.48	$69^{+28}_{-36} \pm 8$		
2.10	$482^{+87}_{-100} \pm 34$	2.80	$65^{+40}_{-47} \pm 11$	3.50	$48^{+21}_{-30} \pm 8$		
2.12	$590^{+95}_{-107} \pm 39$	2.82	$28^{+38}_{-44} \pm 11$	3.52	$68^{+28}_{-36} \pm 4$		
2.14	$338^{+79}_{-91} \pm 23$	2.84	$55^{+37}_{-44} \pm 11$	3.54	$34^{+19}_{-29} \pm 2$		
2.16	$435^{+86}_{-94} \pm 31$	2.86	$73^{+41}_{-53} \pm 10$	3.56	$40^{+18}_{-27} \pm 3$		
2.18	$401^{+83}_{-94} \pm 29$	2.88	$27^{+28}_{-40} \pm 9$	3.58	$20^{+19}_{-26} \pm 1$		
2.20	$520^{+85}_{-98} \pm 36$	2.90	$81^{+41}_{-49} \pm 10$	3.60	$59^{+29}_{-35} \pm 4$		
2.22	$227^{+70}_{-79} \pm 19$	2.92	$18^{+32}_{-39} \pm 1$	3.62	$39^{+21}_{-29} \pm 3$		
2.24	$269^{+74}_{-81} \pm 18$	2.94	$107^{+42}_{-53} \pm 7$	3.64	$25^{+21}_{-29} \pm 2$		

be a conservative systematic uncertainty estimate, due to the $M^2_{\rm miss}(\gamma_{\rm ISR}\eta\phi)$ requirement.

Belle measures luminosity with 1.4% precision while the uncertainty of the generator PHOKHARA is less than 0.5% [31]. The $\sigma^{\rm prod}_{\rm ISR}(J/\psi)$ is according to QED calculation [35] and $\Gamma_{e^+e^-}$ of J/ψ decay, which has an uncertainty of 0.5% [34]. The trigger efficiencies for the events surviving the selection criteria are $(97.0 \pm 0.1)\%$ for the $\pi^+\pi^-\pi^0$ mode and $(95.1 \pm 0.1)\%$ for the $\gamma\gamma$ mode according to the trigger simulation. Conservative uncertainties of 1.0% and 1.5% are taken to be the systematic uncertainties in the trigger efficiencies for the $\pi^+\pi^-\pi^0$ mode and $\gamma\gamma$ modes [9,36]. The uncertainties in the ϕ and η branching fractions are calculated according to the world average values [34],

TABLE III. Summary of the systematic uncertainties (%). There is additional systematic uncertainties in determining the $\mathcal{B}[J/\psi \to \eta\phi]$.

Source	$\gamma\gamma$ mode	$\pi^+\pi^-\pi^0$ mode	Common
Particle identification	2.0	4.0	2.0
Tracking	0.7	1.4	0.7
Photon reconstruction	6.0	6.0	6.0
ϕ, η masses and $M^2_{\rm miss}(\eta\phi\gamma_{\rm ISR})$	1.7	1.4	1.4
Luminosity	1.4	1.4	1.4
Generator	0.5	0.5	0.5
$\sigma^{\rm prod}_{\rm ISR}(J/\psi)$	0.5	0.5	0.5
Trigger	1.5	1.0	...
Branching fractions	0.6	0.6	0.6
J/ψ signal fitting	1.8	1.5	...
MC statistics	0.1	0.1	0.1
Sum	6.9	7.3	6.7
Sum for $\mathcal{B}[J/\psi \to \eta\phi]$	7.2	7.9	6.8

which contribute a systematic uncertainty of 0.6%. The statistical uncertainty in the MC determination of the efficiency is 0.1%.

Assuming all these sources are independent and, adding them in quadrature, the total systematic uncertainties in measuring $\mathcal{B}[J/\psi \to \eta\phi]$ are 7.9% for the $\pi^+\pi^-\pi^0$ mode and 7.2% for the $\gamma\gamma$ mode. There are some common uncertainties in the two modes, as listed in Table III. For other uncertainties that have no correlation between two modes, these are first summed in quadrature to obtain δ_i. Then the total independent uncertainty ($\delta_{\rm tot}$) is calculated by $\sqrt{\sum_i(\Delta\varepsilon_i \times \mathcal{B}_i)^2}/\sum_i(\varepsilon_i \times \mathcal{B}_i)$, where $\Delta\varepsilon_i$ equal to $\delta_i \times \varepsilon_i$, i is the ith mode of η decays ($i = \pi^+\pi^-\pi^0, \gamma\gamma$). The value of $\delta_{\rm sys}$ is calculated by $\sqrt{\sum_j(\delta_j)^2 + (\delta_{\rm tot})^2}$ (δ_j designates each common uncertainty mentioned above), and the total systematic uncertainty thereby calculated to be 6.7%, which is common in the cross section measurement and the determinations for $\mathcal{B}[\phi(1680) \to \eta\phi]$, $\Gamma^{e^+e^-}_{\phi(1680)}\mathcal{B}[\phi(1680) \to \eta\phi]$ and the upper limit of $\Gamma^{e^+e^-}_{\phi(2170)}\mathcal{B}[\phi(2170) \to \eta\phi]$.

By changing the fit range to $[1.6, 2.9]$ GeV/c^2, the systematic uncertainty due to the fit range is found to be negligible. To estimate the model dependence of the nonresonant contribution, we use $A^{n.r.}_{\eta\phi}(s) = a_0/s$. The uncertainties in backgrounds from the 2D sidebands are estimated by changing a or b by 1σ and changing the functions used to parametrize them, as mentioned in Sec. IV. Systematic uncertainties in the cross section resulting from different sideband background parametrizations are also shown in Fig. 7; these translate to uncertainties in the number of J/ψ signal events of 1.8% in the $\gamma\gamma$ mode and 1.5% in the $\pi^+\pi^-\pi^0$ mode. The uncertainty in $\mathcal{B}^{KK^*(892)}_{\phi(1680)}/\mathcal{B}^{\eta\phi}_{\phi(1680)}$ is obtained by varying 1σ according to the previous measurement [24].

VII. SUMMARY

In summary, the $e^+e^- \to \eta\phi$ cross sections are measured from threshold to 3.95 GeV, and no significant $\phi(2170)$ signal is observed. The branching fraction of $J/\psi \to \eta\phi$ is measured to be $(7.2 \pm 0.8 \pm 0.5) \times 10^{-4}$, which is in good agreement with the world average value [34]. There are two solutions with the same fit quality but different phase angles, obtained from fitting the invariant mass distributions of $\eta\phi$ including $\phi(1680)$ but no $\phi(2170)$. The resonant parameters of $\phi(1680)$ are obtained to be $m_{\phi(1680)} = (1696 \pm 8 \pm 10)$ MeV/c^2, $\Gamma_{\phi(1680)} = (175 \pm 13 \pm 16)$ MeV, $\Gamma^{e^+e^-}_{\phi(1680)}\mathcal{B}[\phi(1680) \to \eta\phi] = (75 \pm 10 \pm 11)$ eV or $(207 \pm 16 \pm 20)$ eV, and $\mathcal{B}[\phi(1680) \to \eta\phi] = (25 \pm 12 \pm 2)\%$ or $(23 \pm 10 \pm 2)\%$ for the two solutions. The $\phi(2170)$ signal is not significant, and the upper limit on the $\phi(2170)$ production is determined to be $\Gamma^{e^+e^-}_{\phi(2170)}\mathcal{B}[\phi(2170) \to \eta\phi] < 0.17$ eV or < 18.6 eV at 90% CL; both are consistent with the BESIII measurement [27].

ACKNOWLEDGMENTS

This work, based on data collected using the Belle detector, which was operated until June 2010, was supported by the Ministry of Education, Culture, Sports, Science, and Technology (MEXT) of Japan, the Japan Society for the Promotion of Science (JSPS), and the Tau-Lepton Physics Research Center of Nagoya University; the Australian Research Council including Grants No. DP180102629, No. DP170102389, No. DP170102204, No. DE220100462, No. DP150103061, and No. FT130100303; Austrian Federal Ministry of Education, Science and Research (FWF) and FWF Austrian Science Fund No. P 31361-N36; the National Natural Science Foundation of China under Contracts No. 11675166, No. 11705209; No. 11975076; No. 12135005; No. 12175041; and No. 12161141008; Key Research Program of Frontier Sciences, Chinese Academy of Sciences (CAS), Grant No. QYZDJ-SSW-SLH011; the Ministry of Education, Youth and Sports of the Czech Republic under Contract No. LTT17020; the Czech Science Foundation Grant No. 22-18469S; Horizon 2020 ERC Advanced Grant No. 884719 and ERC Starting Grant No. 947006 "InterLeptons" (European Union); the Carl Zeiss Foundation, the Deutsche Forschungsgemeinschaft, the Excellence Cluster Universe, and the VolkswagenStiftung; the Department of Atomic Energy (Project Identification No. RTI 4002) and the Department of Science and Technology of India; the Istituto Nazionale di Fisica Nucleare of Italy; National Research Foundation (NRF) of Korea Grants No. 2016R1D1A1B02012900,

No. 2018R1A2B3003643, No. 2018R1A6A1A06024970, No. RS202200197659, No. 2019R1I1A3A01058933, No. 2021R1A6A1A03043957, No. 2021R1F1A1060423, No. 2021R1F1A1064008, and No. 2022R1A2C1003993; Radiation Science Research Institute, Foreign Large-size Research Facility Application Supporting project, the Global Science Experimental Data Hub Center of the Korea Institute of Science and Technology Information and KREONET/GLORIAD; the Polish Ministry of Science and Higher Education and the National Science Center; the Ministry of Science and Higher Education of the Russian Federation, Agreement No. 14.W03.31.0026, and the HSE University Basic Research Program, Moscow; University of Tabuk research Grants No. S-1440-0321, No. S-0256-1438, and No. S-0280-1439 (Saudi Arabia); the Slovenian Research Agency Grants No. J1-9124 and No. P1-0135; Ikerbasque, Basque Foundation for Science, Spain; the Swiss National Science Foundation; the Ministry of Education and the Ministry of Science and Technology of Taiwan; and the United States Department of Energy and the National Science Foundation. These acknowledgements are not to be interpreted as an endorsement of any statement made by any of our institutes, funding agencies, governments, or their representatives. We thank the KEKB group for the excellent operation of the accelerator; the KEK cryogenics group for the efficient operation of the solenoid; and the KEK computer group and the Pacific Northwest National Laboratory (PNNL) Environmental Molecular Sciences Laboratory (EMSL) computing group for strong computing support; and the National Institute of Informatics, and Science Information NETwork 6 (SINET6) for valuable network support.

[1] For a review, see S. L Olsen, T. Skwarnichi, and D. Zieminska, Rev. Mod. Phys. **90**, 015003 (2018).
[2] S. Choi *et al.* (Belle Collaboration), Phys. Rev. Lett. **91**, 262001 (2003).
[3] M. Ablikim *et al.* (BESIII Collaboration), Phys. Rev. Lett. **110**, 252001 (2013); Z. Q. Liu *et al.* (Belle Collaboration), Phys. Rev. Lett. **110**, 252002 (2013).
[4] M. Ablikim *et al.* (BESIII Collaboration), Phys. Rev. Lett. **111**, 242001 (2013).
[5] X. L. Wang *et al.* (Belle Collaboration), Phys. Rev. D **91**, 112007 (2015).
[6] M. Ablikim *et al.* (BESIII Collaboration), Phys. Rev. D **96**, 032004 (2017).
[7] B. Aubert *et al.* (*BABAR* Collaboration), Phys. Rev. Lett. **95**, 142001 (2005).
[8] B. Aubert *et al.* (*BABAR* Collaboration), Phys. Rev. D **74**, 091103 (2006).
[9] C. P Shen *et al.* (Belle Collaboration), Phys. Rev. D **80**, 031101 (2009).
[10] G. J. Ding and M. L. Yan, Phys. Lett. B **657**, 49 (2007); Q. Li, L.-C. Gui, M.-S. Liu, Q.-F. Lü, and X.-H. Zhong, Chin. Phys. C **45**, 023116 (2021).
[11] T. Barnes, N. Black, and P. R. Page, Phys. Rev. D **68**, 054014 (2003).
[12] G. J. Ding and M. L. Yan, Phys. Lett. B **650**, 390 (2007).
[13] P. R. Page, E. S. Swanson, and A. P. Szczepaniak, Phys. Rev. D **59**, 034016 (1999).
[14] Z. G. Wang, Nucl. Phys. **A79**, 1106 (2007).
[15] H. X. Chen, X. Liu, A. Hosaka, and S. L. Zhu, Phys. Rev. D **78**, 034012 (2008).
[16] E. Klemp and A. Zaitsev, Phys. Rep. **454**, 1 (2007).
[17] C. F. Qiao, Phys. Lett. B **639**, 263 (2006).
[18] Y. Dong, A. Faessler, T. Gutsche, Q. Lu, and V. E. Lyubovitskij, Phys. Rev. D **96**, 074027 (2017).
[19] Y. L. Yang, D. Y. Chen, and Z. Lu, Phys. Rev. D **100**, 073007 (2019).
[20] S. L. Zhu, Int. J. Mod. Phys. A **E17**, 283 (2008).
[21] A. M. Torres, K. P. Khemchandani, L. S. Geng, M. Napsuciale, and E. Oset, Phys. Rev. D **78**, 074031 (2008).
[22] Y. H. Ma, Y. Chen, M. Gong, and Z. F. Liu, Chin. Phys. C **45**, 013112 (2021).
[23] B. Aubert *et al.* (*BABAR* Collaboration), Phys. Rev. D **76**, 092005 (2007).
[24] B. Aubert *et al.* (*BABAR* Collaboration), Phys. Rev. D **77**, 092002 (2008).
[25] V. L. Ivanov *et al.*, Phys. Lett. B **798**, 134946 (2019).
[26] M. Ablikim *et al.* (BESIII Collaboration), Phys. Rev. D **102**, 012008 (2020).
[27] M. Ablikim *et al.* (BESIII Collaboration), Phys. Rev. D **104**, 032007 (2021).
[28] A. Abashian *et al.* (Belle Collaboration), Nucl. Instrum. Methods Phys. Res., Sect. A **479**, 117 (2002); also see detector section in J. Brodzicka *et al.*, Prog. Theor. Exp. Phys. **2012**, 04D001 (2012).
[29] S. Kurokawa and E. Kikutani, Nucl. Instrum. Methods Phys. Res., Sect. A **499**, 1 (2003), and other papers included in this Volume; T. Abe *et al.*, Prog. Theor. Exp. Phys. **2013**, 03A001 (2013) and references therein.
[30] A. Keshavarzi, D. Nomura, and T. Teubner, Phys. Rev. D **97**, 114025 (2018).
[31] G. Rodrigo, H. Czyż, J. H. Kühn, and M. Szopa, Eur. Phys. J. C **24**, 71 (2002). For a review on the generator,see: S. Actis *et al.*, Eur. Phys. J. C **66**, 585 (2010).
[32] R. Brun *et al.*, GEANT3.21, CERN DD/EE/84-1, 1984.
[33] E. Nakano, Nucl. Instrum. Methods Phys. Res., Sect. A **494**, 402 (2002).
[34] P. A. Zyla *et al.* (Particle Data Group), Prog. Theor. Exp. Phys. **2020**, 083C01 (2020) and 2021 update.
[35] E. A. Kuraev and V. S. Fadin, Yad. Fiz. **41**, 733 (1985) [Sov. J. Nucl. Phys. **41**, 466 (1985)].
[36] X. L. Wang *et al.* (Belle Collaboration), Phys. Rev. D **87**, 051101 (2013).